Boise State University
ScholarWorks

Materials Science and Engineering Faculty Publications and Presentations

Department of Materials Science and Engineering

5-1-2018

Self-Assembly of (111)-Oriented Tensile-Strained Quantum Dots by Molecular Beam Epitaxy

Christopher F. Schuck
Boise State University

Robin A. McCown
Boise State University

Ashlie Hush
Boise State University

Austin Mello
Boise State University

Simon Roy
Boise State University

See next page for additional authors

Copyright (2018) American Institute of Physics on behalf of AVS - Science and Technology of Materials, Interfaces, and Processing. This article may be downloaded for personal use only. Any other use requires prior permission of the author and the American Institute of Physics. The following article appeared in:
Schuck, C. F., McCown, R. A., Hush, A., Mello, A., Roy, S., Spinuzzi, J. W., . . . Simmonds, P. J. (2018). Self-Assembly of (111)-Oriented Tensile-Strained Quantum Dots by Molecular Beam Epitaxy. *Journal of Vacuum Science & Technology B, 36*(3), 031803
and may be found at doi: 10.1116/1.5018002

Authors
Christopher F. Schuck, Robin A. McCown, Ashlie Hush, Austin Mello, Simon Roy, Joseph W. Spinuzzi, and Paul J. Simmonds

This article is available at ScholarWorks: https://scholarworks.boisestate.edu/mse_facpubs/343

Self-assembly of (111)-oriented tensile-strained quantum dots by molecular beam epitaxy

Christopher F. Schuck,[a)] Robin A. McCown, Ashlie Hush, and Austin Mello
Micron School of Materials Science and Engineering, Boise State University, 1910 University Drive, Boise, Idaho 83725

Simon Roy and Joseph W. Spinuzzi
Physics Department, Boise State University, 1910 University Drive, Boise, Idaho 83725

Baolai Liang and Diana L. Huffaker
California NanoSystems Institute, University of California, 570 Westwood Plaza, Los Angeles, California 90095

Paul J. Simmonds
Micron School of Materials Science and Engineering, Boise State University, 1910 University Drive, Boise, Idaho 83725 and Physics Department, Boise State University, 1910 University Drive, Boise, Idaho 83725

(Received 2 December 2017; accepted 12 March 2018; published 30 March 2018)

The authors report on a comprehensive study of the growth of coherently strained GaAs quantum dots (QDs) on (111) surfaces via the Stranski–Krastanov (SK) self-assembly mechanism. Recent reports indicate that the long-standing challenges, whereby the SK growth mechanism could not be used to synthesize QDs on (111) surfaces, or QDs under tensile strain, have been overcome. However, a systematic study of the SK growth of (111)-oriented, tensile-strained QDs (TSQDs) as a function of molecular beam epitaxy growth parameters is still needed. Here, the authors explore the effects of deposition amount, substrate temperature, growth rate, and V/III flux ratio on the SK-driven self-assembly of GaAs(111)A TSQDs. The authors highlight aspects of TSQD SK self-assembly on (111) surfaces that appear to differ from the SK growth of traditional compressively strained QDs on (100) surfaces. The unique properties of (111) QDs and tensile-strained QDs mean that they are of interest for various research areas. The results discussed here offer a practical guide for tailoring the size, shape, density, uniformity, and photon emission wavelength and intensity of (111) TSQDs for future applications. *Published by the AVS.* https://doi.org/10.1116/1.5018002

I. INTRODUCTION

Quantum dots (QDs) are a well-established research area in solid-state optoelectronics;[1,2] their broad utility is limited mainly by the number of material systems from which they can be synthesized. QDs grown on (111) surfaces, and QDs that form under tensile strain, are predicted to have interesting properties stemming from their fundamental physics.[3–7] However, the growth of (111)-oriented, or tensile-strained QDs (TSQDs) via the well-established Stranski–Krastanov (SK) mechanism is known to be extremely challenging, due to the rapid relaxation of strain via dislocations.[1,8–12] We recently reported a solution to this problem. SK self-assembly, the (111) orientation, and tensile strain form an interdependent triad. Together they permit the growth of tensile-strained QDs on (111) surfaces.[3,13,14] Here, we consider these three components in turn.

A. SK self-assembly

SK self-assembly in solid-state semiconductor media by molecular beam epitaxy (MBE) produces high-purity, dislocation-free QDs with precise control of materials, interfaces, and optoelectronic properties,[1,2,15,16] for a wide range of applications.[17–19] QD self-assembly via the SK mechanism is often preferred because of its simplicity, single-step nature, scalability, and controllability via well-understood growth parameters.

B. (111) orientation

QDs grown on low-index planes other than the traditional (100) surface are expected to have unique properties.[3,5–7] The threefold rotational symmetry of zinc blende (111) surfaces are ideal for integration with materials with similar symmetry such as certain topological insulators and 2D materials.[20,21] Furthermore, with inherently low fine structure splitting, QDs grown on a (111) surface are expected to be efficient emitters of polarization entangled photons for quantum optics applications.[5,6,22] Unfortunately, compressive strain relaxes rapidly on this surface, producing periodic networks of misfit dislocations.[1,8–10] Without the presence of strain to drive self-assembly, SK growth of (111) QDs is not possible.[1,15,16] As a result, researchers have developed techniques to side-step SK self-assembly, such as droplet epitaxy (DE) and overgrowth on prepatterned surfaces.[23–26] These techniques bring their own advantages, but can also introduce unwanted defects or require labor-intensive processing steps.[23–26]

C. Tensile strain

In traditional QDs, a smaller lattice constant barrier material surrounds a larger lattice constant QD material, generating compressive strain. Tensile-strained self-assembly would

[a)]Electronic mail: christopherschuck@boisestate.edu

allow us to interchange these lattice constant requirements, which in principle doubles the number of material combinations available for QD self-assembly. Tensile strain also reduces the electronic bandgap, in contrast with the increase in bandgap caused by both compressive strain *and* quantum confinement,[3,27,28] providing exceptionally tunable photonic properties. Promising applications for tensile-strained QDs could therefore include infrared optoelectronics, semiconductor-to-semimetal conversion for high-conductivity tunnel junctions,[29] transformation of Ge into a direct bandgap semiconductor,[4,30] and strain-enhanced thermoelectrics.[31] Inducing tensile strain in QD materials can be challenging, with defects generated at low strains, and the frequent need for complex postgrowth processing.[32,33] An attractive alternative would be to create highly localized nanoscale regions of tensile strain in a single step, just like the compressive strain fields surrounding traditional QDs.[34]

Bringing these three components together, we recently demonstrated that the SK self-assembly of tensile-strained QDs *is* in fact possible, as long as we also change the surface orientation from (100) to (111), or (110).[3,13,14,27,35] The resulting tensile strain-driven self-assembly process is entirely analogous to the mechanism by which QDs form under compressive strain on (100) surfaces.[13,27] In both compressively strained (100) QDs and tensile-strained (111) QDs, atomic arrangement and strain direction interact to favor the formation of dislocation-free QDs.[11–14,36] Although those initial experiments served to confirm many of the expected benefits from the SK self-assembly of (111)-oriented TSQDs, to date there has been no comprehensive study of their growth. To exploit their full potential, it is critical that we fully understand how to tailor their unique properties. To this end, this paper describes a systematic analysis of TSQD growth.

II. EXPERIMENTAL SETUP AND METHODOLOGY

We grew several series of samples using solid-source MBE. Each series represents a variation in the growth parameters for TSQD formation. We determine deposition thickness, in MLs, and growth rate, in MLs per second, using *in situ* reflection high-energy electron diffraction (RHEED) intensity oscillations on the (100) surface, correcting for the differences in areal density and interplanar spacing of the (111) surface. We determine substrate growth temperature, T_{SUB}, using a pyrometer and a substrate-mounted thermocouple that we calibrate using RHEED to observe known phase transitions in sample surface reconstructions. We infer growth fluxes for V/III ratios from the beam equivalent pressure (BEP) measured with a beam flux monitor in front of the substrate heater. Our group V species is As_4 rather than As_2, for consistency with historical research on the (111) surface before As crackers were widely available. We use *ex situ* single crystal x-ray diffraction to calibrate $In_{0.52}Al_{0.48}As$ and $In_{0.53}Ga_{0.47}As$ compositions for lattice-matching to the nominally on-axis InP(111)A substrates.

We measure TSQD shape, size, and areal density with atomic force microscopy (AFM). To calculate TSQD volume, we model them as tetrahedra with an equilateral triangle base, using in-plane and height dimensions taken from our AFM measurements. We measure TSQD emission wavelength and intensity profiles using low-temperature (7 K) photoluminescence (PL). Since the thickness and composition of the InAlAs buffer is nominally identical in all samples, we normalize our PL spectra to the intensity of the InAlAs emission peak. This allows us to compare TSQD *peak PL intensity* (the highest intensity emission at a single QD emission wavelength) across samples. Peak PL intensity is useful for determining the efficiency of QDs emitting at the most common wavelength. However, when PL intensity is lower, simply measuring peak intensity does not allow one to distinguish between broadening of the TSQD size distribution (i.e., fewer TSQDs emitting at the peak wavelength), or reduced TSQD crystal quality due to dislocations (i.e., fewer optically active TSQDs emitting at all wavelengths including at the peak). Plotting *total PL emission* (integrated area of TSQD spectral features) versus QD areal density allows us to make this distinction by providing an indication of *PL emission efficiency* (the relative percentage of QDs that emit light, normalized to the highest value obtained) and, therefore, QD crystal quality.

Our samples consist of GaAs TSQDs grown within $In_{0.52}Al_{0.48}As$ barriers, generating 3.8% tensile strain in the GaAs. The wider bandgap of the InAlAs creates type-I confinement of charge carriers to create optically active GaAs TSQDs.[3,27] Each sample contains both buried and surface TSQDs for optical and structural analysis, respectively. We mount the InP (111)A substrates on molybdenum blocks using indium solder. We grow 50 nm of lattice-matched InGaAs between the InP substrate and the bottom InAlAs barrier (T_{SUB}: 510 °C, growth rate: 169 nm/h, and V/III ratio: 160) for a smoother InAlAs morphology.[7] The bottom InAlAs barrier in all samples is 200 nm thick (T_{SUB}: 510 °C, growth rate: 172 nm/h, and V/III ratio: 160) to minimize surface roughness.[7] The 50 nm InAlAs top barrier is grown in two steps. First, we deposit 10 nm InAlAs at the TSQD growth temperature (growth rate: 172 nm/h, and V/III ratio: 160), to prevent annealing or degradation of the TSQDs, followed by 40 nm InAlAs grown at T_{SUB}: 510 °C (growth rate: 172 nm/h, and V/III ratio: 160). Consistent with previous reports,[27] during TSQD formation we see no change in the RHEED pattern from the streaky (2×2) surface reconstruction of the (111) surface. We attribute the lack of a "spotty" RHEED pattern to the very low areal densities and low height profiles of the GaAs/InAlAs(111)A TSQDs.

Our control for these experiments consists of a sample containing 3.5 ML GaAs TSQDs grown under the following conditions: T_{SUB}: 485 °C, GaAs growth rate: 0.075 ML/s, and As_4/Ga BEP ratio: 75. In each sample series, we adjust a single growth parameter: GaAs deposition thickness: 0–4.5 ML, T_{SUB}: 460–535 °C, GaAs growth rate: 0.025–0.125 ML/s, and As_4/Ga BEP ratio: 50–110.

III. RESULTS AND DISCUSSION

We analyze AFM images taken at multiple positions on each sample to determine TSQD areal density (cm^{-2}), and

average height (nm), diameter (nm), and volume (nm^3). The PL emission wavelengths and intensities we report below come from the highest intensity TSQD peak in each PL spectrum. To explore the effect of MBE growth conditions on TSQD crystal quality, we compare the width of each TSQD size distribution with its corresponding PL emission intensity profile.

A. Deposition amount series

Deposition of <2.5 ML GaAs on InAlAs(111)A, creates a 2D wetting layer that consists of rounded "hills" with ML-high contours [root mean squared (RMS) surface roughness of 0.54 nm] [Fig. 1(a)].

At 2.5 ML, the wetting layer surface becomes rougher (RMS = 0.82 nm). Proto-TSQDs begin to appear that are 1 ML in height (0.33 nm) and 30–50 nm in diameter. These proto-TSQDs nucleate preferentially around the edges of the contoured hills where step-edge density is highest [Fig. 1(b)]. We have seen clustering of TSQDs at step edges in other low-index non-(100) growths,[35] and attribute this effect to longer adatom diffusion lengths compared to the (100) surface,[13] as well as the enhanced accumulation of material at step edges due to the presence of a Schwoebel barrier.[37,38]

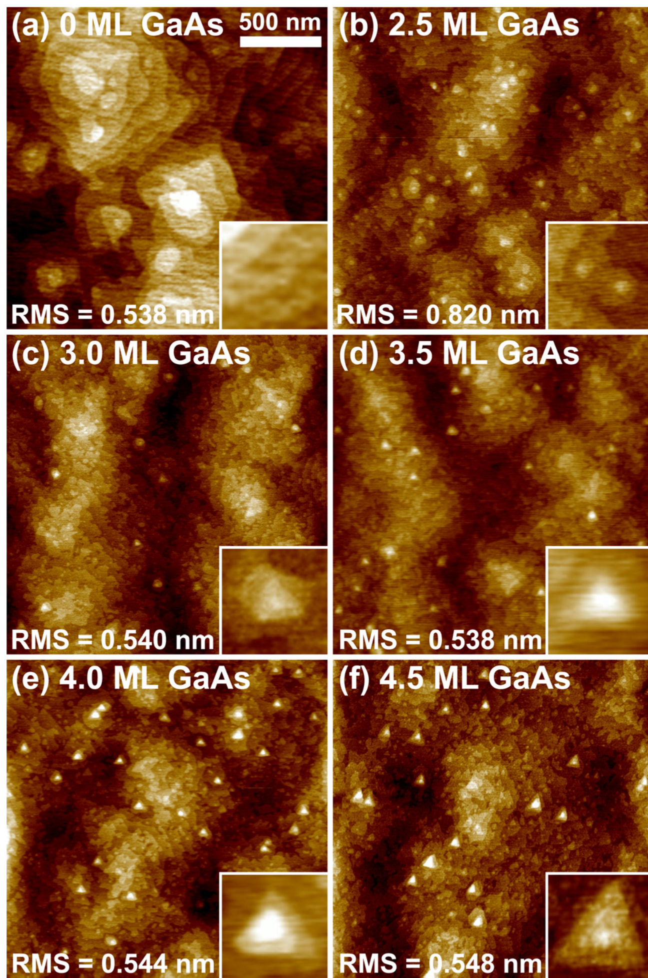

FIG. 1. (Color online) AFM images of 2 × 2 μm^2 with increasing deposition amount: (a) 0 ML, (b) 2.5 ML, (c) 3.0 ML, (d) 3.5 ML, (e) 4.0 ML, and (f) 4.5 ML. Insets are 200 nm^2 (a) and (b), and 100 nm^2 (c)–(f). Proto-TSQDs nucleate by 2.5 ML, then from 3 to 4 ML, both size and areal density of the triangular TSQDs increases. By 4.5 ML TSQD size continues to increase, while areal density begins to decrease.

At 3.0 ML, triangular GaAs TSQDs appear, demarcating the completion of the SK transition from 2D to 3D growth [Fig. 1(c)]. As we increase GaAs deposition from 3.0 to 4.5 ML, the TSQDs grow monotonically in average height, diameter, and volume [Figs. 1(c)–1(f)] (Table I). The only significant change in RMS roughness across this series occurs at 2.5 ML, corresponding to the onset of TSQD nucleation. TSQD volume increases linearly with deposition amount, consistent with the SK growth mode (Table I).

In Table I, average TSQD height, diameter, and volume (with standard deviations), and areal density are determined from AFM images. PL results are determined as described in Sec. II. TSQD height, diameter, volume, and peak PL wavelength all increase with higher deposition amount. TSQD areal density and total PL emission both increase until 4 ML, then decrease at 4.5 ML, resulting in little variation in emission efficiency. These PL results are consistent with quantum confinement effects and sustained crystal quality with increasing deposition amount.

TSQD height and volume distributions broaden with increasing deposition amount (Table I). We attribute this broadening to the appearance of a bimodal TSQD size distribution as the result of Ostwald ripening. A secondary population of TSQDs forms with volume >850 nm^3 (Fig. 2). For the 4.0 and 4.5 ML samples, this secondary population of larger TSQDs represents a significant proportion of the total TSQD population (2% at 3 ML, 4% at 3.5 ML, 13% at 4 ML, and 26% at 4.5 ML). TSQD areal densities are 2 orders of magnitude lower ($\sim 10^8$ cm^{-2}) than typically seen in compressively strained (100)-QDs ($\sim 10^{10}$ cm^{-2}).[39,40] TSQD areal density increases monotonically until 4.0 ML, then decreases at 4.5 ML, providing additional evidence for the onset of Ostwald ripening.

PL from the GaAs TSQDs is significantly red-shifted compared to the emission at 816 nm we measure for unstrained bulk GaAs at 7 K [black dashed line in Fig. 3(a)], confirming that the tensile strain has reduced the TSQD

TABLE I. Deposition amount series characterization statistics [T_{SUB}, growth rate, and V/III ratio held constant (see Sec. II)].

	3.0 ML	3.5 ML	4.0 ML	4.5 ML
Height (nm)	0.85 ± 0.18	0.96 ± 0.23	1.23 ± 0.24	1.21 ± 0.29
Diameter (nm)	44 ± 10	46 ± 11	46 ± 10	53 ± 11
Volume (nm^3)	347 ± 188	419 ± 224	531 ± 280	675 ± 307
Areal density (cm^{-2})	2.8×10^8	5.9×10^8	9.3×10^8	5.6×10^8
Peak PL wavelength (nm)	961	992	1015	1047
Peak PL intensity (a.u.)	0.84	1.05	1.37	0.82
Total PL emission (a.u.)	57.5	83.6	117.4	81.2
Emission efficiency (a.u.)	23.9	16.6	14.4	16.7

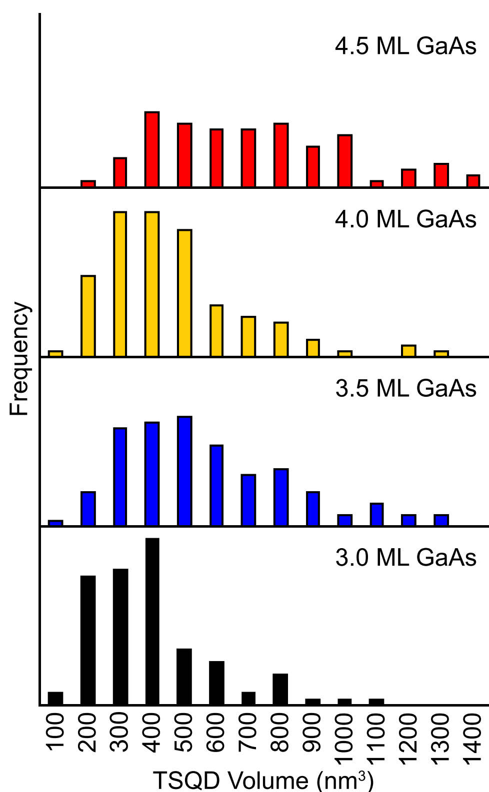

FIG. 2. (Color online) Average TSQD volume histogram with increasing deposition amount. Average TSQD volume from 3.0 to 4.5 ML deposition has a consistent peak from 300 to 500 nm^3. With increasing deposition amount, a secondary population of >800 nm^3 volume TSQDs becomes more apparent. By 4.0 and 4.5 ML, this larger secondary population represents a significant portion of the TSQDs.

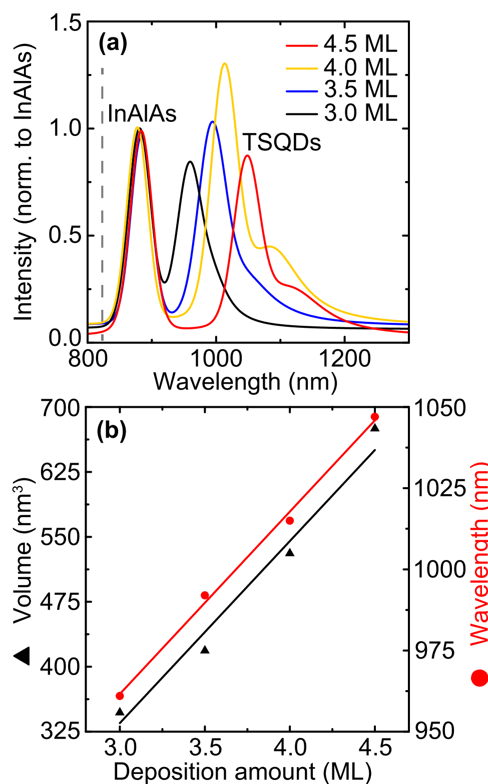

FIG. 3. (Color online) (a) PL emission spectra as a function of GaAs deposition amount in ML. Black dashed line shows 7 K PL emission of unstrained bulk GaAs for comparison. Peak TSQD PL wavelength increases with higher deposition amount up to 4.0ML, then decreases at 4.5 ML. By 3.5 ML a background of longer wavelength emission is apparent, which resolves into a secondary peak for 4.0 and 4.5 ML deposition. Spectral intensities are normalized to the bulk InAlAs PL peak. (b) TSQD volume and peak PL wavelength as a function of GaAs deposition amount. TSQD volume and PL wavelength both increase linearly with increasing deposition amount.

bandgap. The PL wavelength increases as the TSQDs get larger, due to the reduction of the confined ground state energy. Across this series, TSQD PL wavelength is linearly tunable from 961 to 1047 nm by increasing the GaAs deposition amount. This wavelength increase corresponds to a reduction in the TSQD ground state transition energy from 1.29 to 1.18 eV. This PL red-shift correlates with increasing TSQD volume, confirming that it arises from quantum size effects [Fig. 3(b)].

PL emission intensity increases in this series for 3.0–4.0 ML TSQDs, then decreases at 4.5 ML. A longer-wavelength shoulder on the TSQD peak appears at 3.5 ML, which develops into a secondary, longer-wavelength peak in the 4.0 and 4.5 ML sample spectra. This additional spectral feature corresponds to emission from a population of larger TSQDs, confirming the bimodal evolution of TSQD size we observed with AFM analysis.

In the 3.0–4.0 ML range, peak PL intensity increases linearly with TSQD areal density. At 4.5 ML, both peak PL intensity and TSQD density decrease, although the decrease in peak PL intensity is disproportionately large. To rule out dislocation nucleation in large Ostwald-ripened QDs as the cause of this reduction in PL intensity, we performed plan-view transmission electron microscopy (TEM) (not shown here). We found no evidence of dislocations in the 4.5 ML TSQDs, a result that is consistent with previous analysis of TSQDs with TEM.[3,14] This finding is supported by the relatively constant PL emission efficiency with increasing deposition amount (Table I), again suggesting no deterioration in crystal quality for the 4.5 ML sample.

B. Substrate temperature (T_{SUB}) series

As we increase T_{SUB} for the growth of 3.5 ML GaAs TSQDs, we initially see a decrease in TSQD volume in the range 460–485 °C (Table II). Kinetic Monte Carlo simulations of kinetic versus thermodynamic control of island nucleation and growth suggest that thermodynamic control could be the cause of this observed decrease in TSQD volume with increasing T_{SUB}.[41] However, at higher T_{SUB} in the range 485–535 °C, average TSQD volume is essentially constant (Table II), varying less than one standard deviation about an average value (437 ± 213 nm^3). This volume saturation in the face of decreasing aspect ratio (see below) perhaps suggests that TSQD volume has reached thermodynamic equilibrium.[41] We discuss this topic further in Sec. III C.

In Table II, average TSQD height, diameter, and volume (with standard deviations), and areal density are determined from AFM images. PL results are determined as described in Sec. II. TSQD height and volume both decrease from 460 to 485 °C. Peak PL wavelength is constant throughout,

TABLE II. Substrate temperature (T_{SUB}) series characterization statistics [deposition amount, growth rate, and V/III ratio held constant (see Sec. II)].

	460 °C	485 °C	510 °C	535 °C
Height (nm)	1.29 ± 0.31	0.96 ± 0.23	0.73 ± 0.20	0.74 ± 0.18
Diameter (nm)	50 ± 10	46 ± 11	54 ± 9	55 ± 8
Volume (nm^3)	633 ± 284	419 ± 224	436 ± 220	456 ± 193
Areal density (cm^{-2})	5.3×10^8	5.9×10^8	9.6×10^8	4.9×10^8
Peak PL wavelength (nm)	982	992	974	978
Peak PL intensity (a.u.)	0.49	1.05	1.96	2.50
Total PL emission (a.u.)	36.2	83.6	165.6	208.5
Emission efficiency (a.u.)	7.8	16.3	19.7	48.8

despite the initial volume decrease. Total PL emission increases monotonically with T_{SUB}, despite TSQD areal density decreasing above 510 °C. Both of these PL phenomena are consistent with improved crystal quality at higher T_{SUB}.

We can change the shape of these 3.5 ML GaAs TSQDs by growing them at higher T_{SUB}. Raising T_{SUB} from 460 to 535 °C reduces the TSQD aspect ratio (height-to-base diameter ratio) from 0.026 to 0.013; their average height decreases while their diameter increases (Table II). Similar temperature-dependent flattening has been previously observed during annealing of QDs grown by DE, where the authors attributed the decrease in aspect ratio to increased adatom diffusion lengths at higher T_{SUB}.[42]

This behavior for TSQDs is quite different from the growth of traditional compressively strained QDs on (100) surfaces. As T_{SUB} increases, QDs typically increase in volume and decrease in areal density, with any morphological changes occurring along indexed facets.[1,40,41] Traditional InAs(100) QDs also tend to have smaller diameters (∼25 nm), and larger heights (∼5 nm) compared with the (111) TSQDs.[1,40,43] InAs(100) QDs therefore have height-to-base aspect ratios (0.200 ± 0.05) that are an order of magnitude larger than those of the TSQDs in this study (0.020 ± 0.007). That the aspect ratio of TSQDs is so small is primarily the result of their very low heights, consisting as they do of monolayer-high steps that we can resolve in AFM [Figs. 1(e)–1(f)]. These results suggest TSQDs may not in fact erupt in a rapid 2D-to-3D SK transition, but instead self-assemble via a more gradual coalescence that is more consistent with a simple adatom diffusion model. A smoother 3D transition is perhaps not surprising. Compared to the (100) surface, the (111)A surface has lower surface energy,[44] and longer adatom diffusion length.[45,46] Lower surface energy reduces the barrier between 2D and 3D growth, while higher adatom diffusion increases the accessibility of low energy sites such as step edges and islands.

The fact that we see TSQD areal density increase as we raise T_{SUB} from 460 to 510 °C, but then decrease by 535 °C (Table II) suggests some dynamic shift in the kinetics or energetics of TSQD formation. This shift results in a sign change in the slope on an Arrhenius plot of the natural logarithm of areal density against 1000/T_{SUB}, possibly indicating a change from kinetic to thermodynamic control,[15,41] or a crossing of the boundary between SK and Volmer–Weber 3D growth modes.[47] We plan additional experiments to distinguish between these mechanisms.

The PL emission wavelength from the TSQDs does not change systematically with T_{SUB}, suggesting little change in volume with increasing T_{SUB} among TSQDs emitting at the peak wavelength (i.e., TSQDs with the most common size) (Table II) [Fig. 4(a)]. That being said, the sample grown at

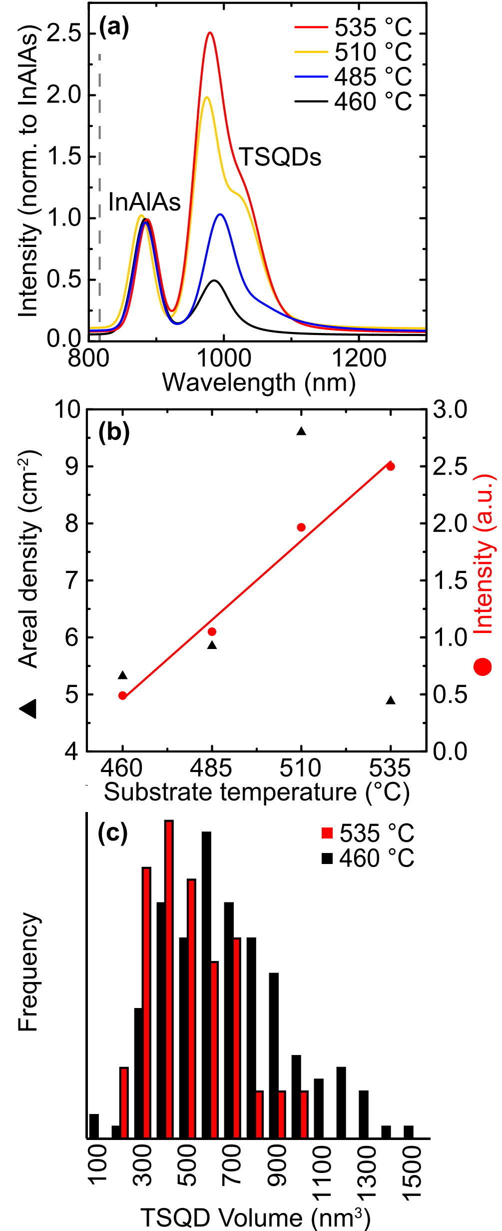

FIG. 4. (Color online): (a) TSQD PL emission as a function of T_{SUB}. As we raise T_{SUB}, peak TSQD PL wavelength remains constant, while peak PL intensity increases. (b) TSQD areal density and peak PL intensity as a function of T_{SUB}. Peak PL intensity increases linearly with T_{SUB}, while TSQD areal density increases up to 510 °C, then decreases at higher T_{SUB}. Increased peak PL intensity at 535 °C, despite a reduction in TSQD areal density, suggests an improvement in crystal quality. (c) Histograms of TSQD volume for the samples grown at lowest (460 °C) and highest (535 °C) T_{SUB}.

460 °C emits at the same wavelength as the three other samples in this series despite having TSQDs with larger average volume (Table II). It is likely that at this low T_{SUB}, the larger TSQDs form dislocations that inhibit their optical activity. Increasing T_{SUB} to 485 °C more than doubles peak PL emission intensity, while TSQD areal density only increases by 11% (Table II). Taken together, these results suggest a dramatic improvement in crystal quality as we raise T_{SUB}. Indeed, peak PL intensity linearly undergoes a five-fold increase as T_{SUB} is raised from 460 to 535 °C (Table II). Plotting areal density against peak PL intensity contrasts the linear increase in intensity with the nonlinear variation in areal density [Fig. 4(b)]. However, as in the ML series, the TSQD size distribution also narrows as peak PL intensity increases (Tables I and II). Comparing areal density to the total PL emission results in the same nonlinearity as for the peak PL intensity. PL emission efficiency is essentially constant across the deposition amount series (Sec. III A) and growth rate series (Sec. III C). For this T_{SUB} series, however, PL emission efficiency more than halves (53% reduction) when cooling from 485 to 460 °C, and triples (199% increase) when heating from 485 to 535 °C. This evidence favors a significant improvement in TSQD crystal quality with T_{SUB}, most likely from a reduction in point defects due to annealing effects at higher temperatures. An enhancement in crystal quality is supported by the fact that we see a slight decrease in surface roughness in AFM as we raise T_{SUB} from 460 °C (RMS = 0.56 nm) to 535 °C (RMS = 0.49 nm).

As with the deposition amount series, average TSQD volume is essentially consistent across this series at 300–600 nm^3 [Fig. 4(c)]. However, all samples also exhibit a population of larger TSQDs (800–1100 nm^3) that we believe is responsible for the longer wavelength shoulder peak at ~1050 nm seen in the PL spectra for samples grown at T_{SUB} ≥485 °C [Fig. 4(b)]. The fact that this shoulder peak is not seen for the sample grown at 460 °C indicates that these larger TSQDs are not optically active at low T_{SUB}. However, the appearance and subsequent increase in relative intensity of the shoulder peak as T_{SUB} is raised, suggests that optical quality of these larger QDs also improves at higher T_{SUB}, just as we have concluded for the majority TSQD population.

TABLE III. Growth rate series characterization statistics [deposition amount, T_{SUB}, and V/III ratio held constant (see Sec. II)].

	0.025 ML/s	0.075 ML/s	0.100 ML/s	0.125 ML/s
Height (nm)	0.88 ± 0.23	0.96 ± 0.23	0.71 ± 0.17	0.82 ± 0.20
Diameter (nm)	59 ± 10	46 ± 11	48 ± 9	49 ± 8
Volume (nm^3)	627 ± 301	419 ± 223	341 ± 179	400 ± 182
Areal density (cm^{-2})	5.2×10^8	5.9×10^8	6.6×10^8	7.6×10^8
Peak PL wavelength (nm)	990	992	998	1004
Peak PL intensity (a.u.)	0.86	1.05	1.11	1.35
Total PL emission (a.u.)	85.6	83.6	98.7	103
Emission efficiency (a.u.)	18.7	16.3	17.2	15.6

C. Growth rate series

As we increase the growth rate for 3.5 ML GaAs TSQDs from 0.025 to 0.075 ML/s, TSQD volume decreases while areal density increases (Table III), consistent with trends seen in traditional QD growth.[48,49] We attribute these trends to the higher population of adatoms on the epitaxial surface per unit time as the growth rate increases, increasing the likelihood that two adatoms meet and nucleate a new island, before they attach to an existing island. However, as we increase GaAs growth rate further, from 0.075 to 0.125 ML/s, average TSQD height, diameter, and volume remain statistically constant (Table III). The higher average volume at 0.025 ML/s is due to a secondary population of larger TSQDs (volume ~700 nm^3) that exists in addition to the primary population with average volume ~400 nm^3 (Fig. 5). As in the T_{SUB} series, this behavior contrasts with traditional QD formation where we would expect a continued reduction in TSQD size and an increase in areal density with increasing growth rate. At higher growth rates, more adatoms are present on the epitaxial surface at any given time; as T_{SUB} is raised, adatom mobility is increased. In both cases, the rate of adatom collisions and interactions increases, but in the case of TSQD growth this does not appear to translate into a change in their average volume.

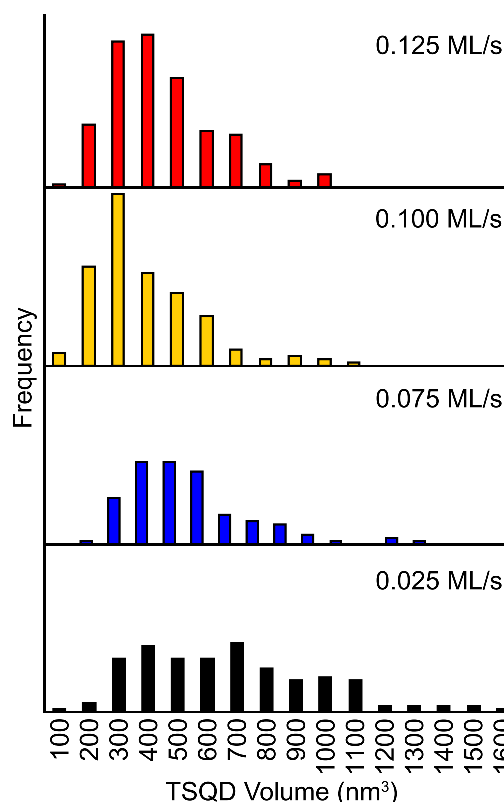

FIG. 5. (Color online) Histograms of average TSQD volume as a function of increasing growth rate. For all samples, we see a consistent peak corresponding to TSQDs with average volume 300–500 nm^3 [as also seen in the ML series (Fig. 2)]. However, for the 0.025 ML/s sample, a broad secondary population >700 nm^3 is also present.

In Table III, the average TSQD height, diameter, and volume (with standard deviations), and areal density are determined from AFM images. PL results are determined as described in Sec. II. TSQD diameter and volume both decrease from 0.025 to 0.075 ML/s. At higher growth rates, TSQD height, diameter, and volume are statistically constant. Peak PL wavelength remains constant throughout, despite the initial volume decrease. Despite a disproportionate increase in peak PL intensity compared to areal density, total PL emission increases linearly with TSQD areal density, resulting in little variation in emission efficiency. These AFM and PL results are consistent with broadening of the TSQD size distribution at lower growth rates.

The average TSQD volume (443 ± 248 nm^3) across all four growth rate samples is very close to the average volume (437 ± 213 nm^3) calculated across the three T_{SUB} samples grown at 485–535 °C (discussed in Sec. III B). In addition, the fact that PL emission wavelength does not change as we tune growth rate [Fig. 6(a)] or T_{SUB} [Fig. 4(a)] provides further evidence for the TSQDs having reached a constant volume. These observations suggest that the GaAs(111)A TSQDs may be attaining an equilibrium size over the growth parameter ranges studied here. QDs are predicted to reach an equilibrium size as the result of competition between two mechanisms. Larger QDs reduce the total surface area compared to many small QDs, and so are energetically favorable (as in Ostwald ripening). However, larger QDs are surrounded by larger elastic strain fields that eventually promote adatom detachment and escape. The balance between these two mechanisms is predicted to lead to QDs with some equilibrium size.[16,40,41,47] Although QDs with equilibrium size have been widely discussed,[1,41,47,50] they are rarely observed in traditional QD material systems, perhaps as a result of lower adatom migration lengths on (100) surfaces compared to (111)A, and the lower T_{SUB} values required to prevent indium desorption when growing InAs QDs. The fact that we see suggestions of equilibrium island size during tensile-strained self-assembly could lead in the future to TSQDs with exceptionally high size uniformity.

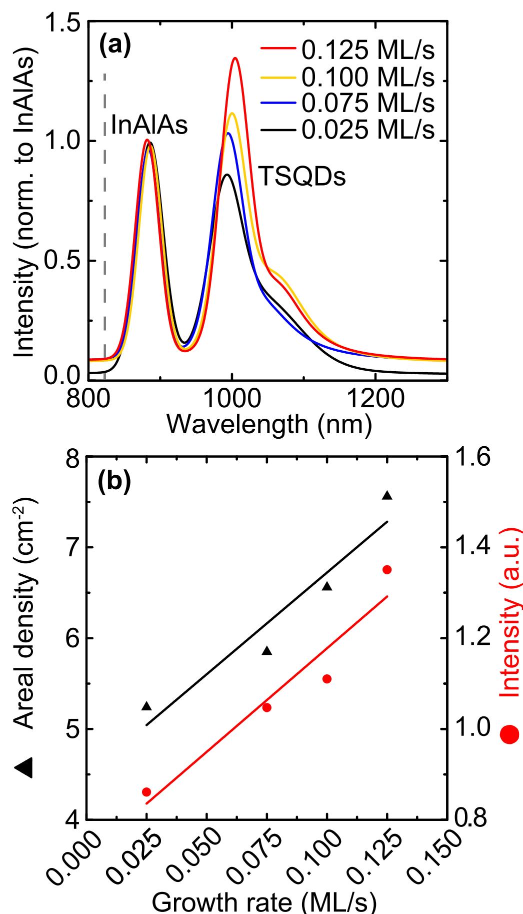

FIG. 6. (Color online): (a) PL emission wavelength and intensity with increasing growth rate. Peak TSQD PL wavelength remains constant with increasing growth rate. Peak PL intensity increases with growth rate. (b) TSQD areal density and peak PL intensity as a function of growth rate. Peak PL intensity and TSQD areal density increase monotonically with growth rate, suggesting that brighter PL emission with growth rate is due to the presence of more TSQD emitters.

To provide additional experimental support for this theory, we performed annealing experiments on our GaAs(111)A TSQDs. If the TSQDs have already reached equilibrium size during growth, we would not expect significant changes in TSQD volume after annealing. Using our standard MBE conditions, we grew a sample with 4.5 ML TSQDs at $T_{SUB} = 522$ °C, and then held the sample at the growth temperature for 5 min under an arsenic flux to anneal the TSQDs. The annealed TSQDs have the same average volume (1344 nm^3) as 4.5 ML TSQDs grown under the same conditions without annealing (1395 nm^3), which lends support to an equilibrium size explanation for our observations. Interestingly, although total TSQD volume remains constant, we do see a reduction in TSQD aspect ratio. A change in aspect ratio is consistent with the trend for samples grown at higher T_{SUB} that we attributed to annealing, helping to confirm that conclusion.

TSQD areal density and PL peak intensity both increase monotonically with increasing growth rate [Fig. 6(b)]. The presence of a secondary TSQD population at a low growth rate therefore accounts for the disparity between TSQD volume and peak wavelength. Areal density versus total PL emission is also linear, resulting in little variation in emission efficiency at different growth rates. Therefore, the increase in the total number of TSQDs at higher growth rate fully accounts for the observed increase in peak PL intensity.

D. V/III ratio series

As we increase the As_4/Ga (V/III) BEP ratio from 50 to 110, the average height, diameter, and volume of the 3.5 ML TSQDs remain statistically constant (Table IV). However, areal density increases exponentially across the same range of V/III ratios (Table IV).

In Table IV, the average TSQD height, diameter, and volume (with standard deviations), and areal density, are determined from AFM images. PL results are determined as described in Sec. II. TSQD height, diameter, volume, and peak wavelength are statistically constant with increasing V/III ratio. With increasing V/III ratio, TSQD areal density increases exponentially, while peak PL intensity decreases

TABLE IV. V/III ratio series characterization statistics [deposition amount, T_{SUB}, and growth rate held constant (see Sec. II)].

	V/III 50	V/III 75	V/III 110
Height (nm)	0.65 ± 0.12	0.96 ± 0.23	0.72 ± 0.22
Diameter (nm)	51 ± 9	46 ± 11	55 ± 11
Volume (nm^3)	337 ± 139	419 ± 223	471 ± 260
Areal density (cm^{-2})	2.1×10^8	5.9×10^8	17.1×10^8
Peak PL wavelength (nm)	982	992	987
Peak PL intensity (a.u.)	3.45	1.05	0.52
Total PL emission (a.u.)	184.2	83.6	110.8
Emission efficiency (a.u.)	100	16.3	7.4

exponentially. These data suggest a significant decrease in crystal quality, confirmed by a substantial reduction in emission efficiency at higher V/III ratio.

Such strong effects on QD areal density are more typically experienced when increasing growth rate,[48] which given the group V rich growth regimes typically adopted for these materials, is determined by the group III flux. That growth rate (varying group III and V flux together) has only a small effect on areal density, while V/III ratio (varying only group V flux) has a large effect, could indicate a group V rate-limiting step.[51] Further, the fact that the observed change in areal density is exponential would mean that for the (111)A surface this rate step is second-order with respect to As_4 flux.[52] Such behavior would mean that TSQD properties are much more sensitive than expected to variations in group V flux. This sensitivity of TSQD formation to As_4 flux is likely related to a kinetic step requiring the bimolecular reaction of As_4 molecules for incorporation, and the additional reaction pathways available due to As_4 dissociation into As_2 dimers.[53–55] This step could be related to a second-order reaction of As_4 with Ga, which is known to occur on the GaAs(100) surface.[56,57] However, the shorter lifetimes of both As_2 and As_4 on (111) surfaces compared with (100) could also play a role.[55,58] To distinguish between these factors, further experiments are planned in which we will explore how As_2 and As_4 impact TSQD formation on (111) surfaces. These experiments must be performed independently for the (111)A and (111)B surfaces due to the differences in surface reconstruction, surface diffusion, and surface energy that result from their termination with either a groups III or V atom.[44,45]

PL measurements for the V/III ratio series provide a striking contrast to the other three series [Fig. 7(a)]. Even as TSQD areal density *increases* exponentially with higher As_4, peak PL intensity *decreases* exponentially [Fig. 7(b)]. A plot of areal density versus total PL emission is nonmonotonic with a dramatic decrease in PL emission efficiency as we increase V/III ratio from 50 to 110. Taken together, these results suggest that the decrease in peak PL intensity is due to defect formation, most likely arsenic antisite defects since these are the most common point defect in GaAs.[59] The fact that we see indications of a reaction rate that is highly sensitive to As flux means V/III ratio must be carefully optimized during the growth of GaAs (111)A TSQDs to maintain crystal quality.

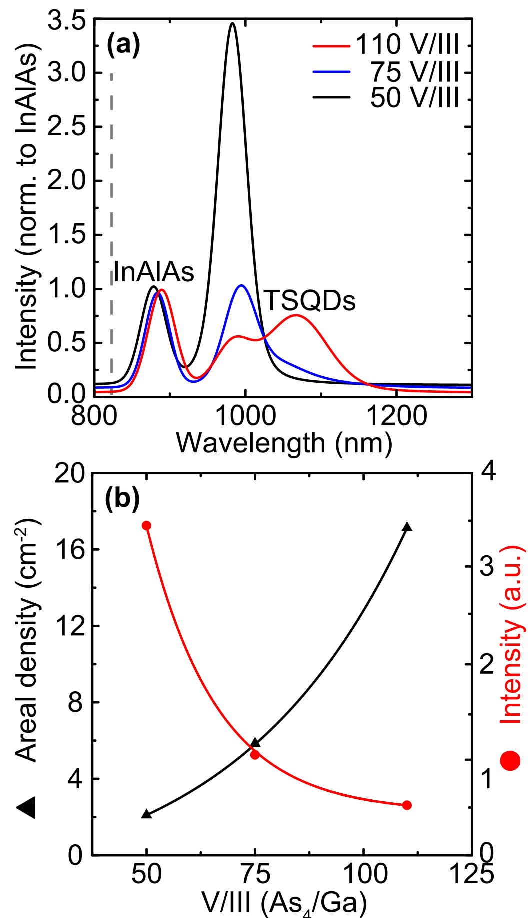

FIG. 7. (Color online) (a) PL emission wavelength and intensity with increasing V/III ratio. Peak TSQD PL wavelength remains constant with increasing growth rate. Peak PL intensity decreases significantly with V/III ratio. (b) TSQD areal density and peak PL intensity as a function of V/III ratio. With increasing V/III ratio, peak PL intensity decreases exponentially, while TSQD areal density increases exponentially, suggesting V/III ratio has a significant effect on crystal quality, possible due to increased As antisite defects at higher As concentrations.

A histogram of TSQD volume (not shown here) indicates that the origin of the longer wavelength PL peak (see particularly the V/III = 110 sample) is a secondary population of larger volume TSQDs. However, comparing the large reduction in TSQD emission efficiency nevertheless confirms significantly reduced crystal quality with increasing V/III ratio (as we saw previously with decreasing T_{SUB}). In the future, we hope to determine whether we can adjust other growth parameters to grow these larger TSQDs with improved crystal quality, since this could be another route by which to tune TSQD emission toward the IR.

IV. SUMMARY AND CONCLUSIONS

We have shown that by manipulating MBE parameters we can reliably control TSQD structural and optical properties. TSQD volume, height, and aspect ratio can all be adjusted consistently. We can also tune TSQD areal density, which is typically low (on the order of $10^8\,cm^{-2}$). PL emission wavelength is tunable with TSQD size and occurs below the bulk bandgap due to the large residual tensile

strain. The results of these experiments posit several interesting possibilities regarding the underlying physics of both (111)-oriented and tensile-strained QD growth.

These experiments reveal two routes by which we expect to obtain brighter TSQD PL emission: (1) using higher growth rates to narrow the QD size distribution; and (2) growing at higher T_{SUB} or lower V/III ratio to improve QD crystal quality. In the future, a TSQD system with higher tensile strain, or a smaller bandgap, could allow us to red-shift PL emission even further for IR applications. The results presented here explicate the use of MBE parameters to adjust the Stranski–Krastanov process, and hence to tailor the structural and optical properties of self-assembled GaAs TSQDs on (111) surfaces. This work provides a comprehensive foundation for research into the growth and applications of these promising nanostructures.

ACKNOWLEDGMENTS

This material is based on work supported by the National Science Foundation under NSF CAREER Grant No. 1555270. The authors also thank Minjoo Larry Lee for useful discussions.

[1]B. A. Joyce and D. D. Vvedensky, Mater. Sci. Eng., R **46**, 127 (2004).
[2]F. Ratto and F. Rosei, Mater. Sci. Eng., R **70**, 243 (2010).
[3]C. D. Yerino *et al.*, Appl. Phys. Lett. **105**, 251901 (2014).
[4]G. Signorello, E. Lörtscher, P. A. Khomyakov, S. Karg, D. L. Dheeraj, B. Gotsmann, H. Weman, and H. Riel, Nat. Commun. **5**, 3655 (2014).
[5]A. Schliwa, M. Winkelnkemper, A. Lochmann, E. Stock, and D. Bimberg, Phys. Rev. B **80**, 161307(R) (2009).
[6]R. Singh and G. Bester, Phys. Rev. Lett. **103**, 063601 (2009).
[7]C. D. Yerino, B. Liang, D. L. Huffaker, P. J. Simmonds, and M. L. Lee, J. Vac. Sci. Technol., B **35**, 010801 (2017).
[8]A. Ohtake, M. Ozeki, and J. Nakamura, Phys. Rev. Lett. **84**, 4665 (2000).
[9]H. Yamaguchi, J. G. Belk, X. M. Zhang, J. L. Sudijono, M. R. Fahy, T. S. Jones, D. W. Pashley, and B. A. Joyce, Phys. Rev. B **55**, 1337 (1997).
[10]H. Yamaguchi, M. R. Fahy, and B. A. Joyce, Appl. Phys. Lett. **69**, 776 (1996).
[11]D. Pachinger, H. Groiss, M. Teuchtmann, G. Hesser, and F. Schäffler, Appl. Phys. Lett. **98**, 223104 (2011).
[12]J. Petruzzello and M. R. Leys, Appl. Phys. Lett. **53**, 2414 (1988).
[13]P. J. Simmonds and M. L. Lee, J. Appl. Phys. **112**, 054313 (2012).
[14]P. J. Simmonds and M. L. Lee, Appl. Phys. Lett. **99**, 123111 (2011).
[15]D. Eaglesham and M. Cerullo, Phys. Rev. Lett. **64**, 1943 (1990).
[16]D. Leonard, M. Krishnamurthy, C. M. Reaves, S. P. Denbaars, and P. M. Petroff, Appl. Phys. Lett. **63**, 3203 (1993).
[17]D. L. Huffaker, G. Park, Z. Zou, O. B. Shchekin, and D. G. Deppe, Appl. Phys. Lett. **73**, 2564 (1998).
[18]H. W. Li, B. E. Kardynał, P. See, A. J. Shields, P. Simmonds, H. E. Beere, and D. A. Ritchie, Appl. Phys. Lett. **91**, 073516 (2007).
[19]P. J. Simmonds, M. Sun, R. B. Laghumavarapu, B. Liang, A. G. Norman, J.-W. Luo, and D. L. Huffaker, Nanotechnology **25**, 445402 (2014).
[20]K. Onomitsu, R. Neufeld, K. Kumakura, and H. Yamamoto, *18th International Conference Molecular Beam Epitaxy*, Flagstaff, AZ (2014), pp. 453–454.
[21]Y. Takagaki and B. Jenichen, Semicond. Sci. Technol. **27**, 035015 (2012).
[22]A. J. Shields, Nat. Photonics **1**, 215 (2007).
[23]G. Juska, E. Murray, V. Dimastrodonato, T. H. Chung, S. Moroni, A. Gocalinska, and E. Pelucchi, J. Appl. Phys. **117**, 134302 (2015).
[24]J. Treu, C. Schneider, A. Huggenberger, T. Braun, S. Reitzenstein, and S. Ho, Appl. Phys. Lett. **101**, 022102 (2012).
[25]E. Stock *et al.*, Appl. Phys. Lett. **96**, 093112 (2010).
[26]T. Mano, M. Abbarchi, T. Kuroda, B. McSkimming, A. Ohtake, K. Mitsuishi, and K. Sakoda, Appl. Phys. Express **3**, 065203 (2010).
[27]P. J. Simmonds, C. D. Yerino, M. Sun, B. Liang, D. L. Huffaker, V. G. Dorogan, Y. Mazur, G. Salamo, and M. L. Lee, ACS Nano **7**, 5017 (2013).
[28]C. D. Yerino *et al.*, Appl. Phys. Lett. **105**, 071912 (2014).
[29]J. M. O. Zide, A. Kleiman-Shwarsctein, N. C. Strandwitz, J. D. Zimmerman, T. Steenblock-Smith, A. C. Gossard, A. Forman, A. Ivanovskaya, and G. D. Stucky, Appl. Phys. Lett. **88**, 162103 (2006).
[30]M. El Kurdi, G. Fishman, Ś. Sauvage, and P. Boucaud, J. Appl. Phys. **107**, 013710 (2010).
[31]X. Li, K. Maute, M. L. Dunn, and R. Yang, Phys. Rev. B **81**, 245318 (2010).
[32]A. Ghrib, M. El Kurdi, M. de Kersauson, M. Prost, S. Sauvage, X. Checoury, G. Beaudoin, I. Sagnes, and P. Boucaud, Appl. Phys. Lett. **102**, 221112 (2013).
[33]J. Greil, A. Lugstein, C. Zeiner, G. Strasser, and E. Bertagnolli, Nano Lett. **12**, 6230 (2012).
[34]A. Lenz, E. Tournie´, J. Schuppang, M. Dähne, and H. Eisele, Appl. Phys. Lett. **102**, 102105 (2013).
[35]P. J. Simmonds and M. L. Lee, Appl. Phys. Lett. **97**, 153101 (2010).
[36]E. P. Kvam and R. Hull, J. Appl. Phys. **73**, 7407 (1993).
[37]H. Lee, R. R. Lowe-Webb, W. Yang, and P. C. Sercel, Appl. Phys. Lett. **71**, 2325 (1997).
[38]R. L. Schwoebel and E. J. Shipsey, J. Appl. Phys. **37**, 3682 (1966).
[39]P. B. Joyce, T. J. Krzyzewski, G. R. Bell, T. S. Jones, S. Malik, D. Childs, and R. Murray, J. Cryst. Growth **227–228**, 1000 (2001).
[40]K. Jacobi, Prog. Surf. Sci. **71**, 185 (2003).
[41]V. Shchukin, E. Scholl, and P. Kratzer, *Semiconductor Nanostructures*, edited by D. Bimberg (Springer, Berlin/Heidelberg/New York, 2008), pp. 1–39.
[42]S. Bietti, L. Esposito, A. Fedorov, A. Ballabio, A. Martinelli, and S. Sanguinetti, Nanoscale Res. Lett. **10**, 247 (2015).
[43]M. C. Xu, Y. Temko, T. Suzuki, and K. Jacobi, J. Appl. Phys. **98**, 083525 (2005).
[44]J. W. Cahn and R. E. Hanneman, Surf. Sci. **1**, 387 (1964).
[45]T. Takebe, M. Fujii, T. Yamamoto, K. Fujita, and T. Watanabe, J. Appl. Phys. **81**, 7273 (1997).
[46]C. Lobo and R. Leon, J. Appl. Phys. **83**, 4168 (1998).
[47]A.-L. Barabási, Mater. Sci. Eng., B **67**, 23 (1999).
[48]P. B. Joyce, T. J. Krzyzewski, G. R. Bell, T. S. Jones, S. Malik, D. Childs, and R. Murray, Phys. Rev. B **62**, 10891 (2000).
[49]H. Dobbs, D. D. Vvedensky, A. Zangwill, J. Johansson, N. Carlsson, and W. Seifert, Phys. Rev. Lett. **79**, 897 (1997).
[50]I. Daruka and A.-L. Barabási, Appl. Phys. Lett. **72**, 2102 (1998).
[51]A. Madhukar, Q. Xie, P. Chen, and A. Konkar, Appl. Phys. Lett. **64**, 2727 (1994).
[52]J. H. Van't Hoff, *Études de Dynamique Chimique [Studies in Chemical Dynamics]* (Frederick Muller, Amsterdam, 1884).
[53]E. S. Tok, J. H. Neave, J. Zhang, B. A. Joyce, and T. S. Jones, Surf. Sci. **374**, 397 (1997).
[54]Y. G. Galitsyn, I. I. Marakhovka, S. P. Moshchenko, and V. G. Mansurov, Tech. Phys. Lett. **24**, 260 (1998).
[55]B. A. Joyce, D. D. Vvedensky, T. S. Jones, M. Itoh, G. R. Bell, and J. G. Belk, J. Cryst. Growth **201/202**, 106 (1999).
[56]C. T. Foxon and B. A. Joyce, Surf. Sci. **64**, 293 (1977).
[57]A. Avery, H. Dobbs, D. Holmes, B. Joyce, and D. Vvedensky, Phys. Rev. Lett. **79**, 3938 (1997).
[58]M. R. Fahy, K. Sato, and B. A. Joyce, Appl. Phys. Lett. **64**, 190 (1994).
[59]H. P. Komsa and A. Pasquarello, Phys. B: Condens. Matter **407**, 2833 (2012).